Additional Study of Water Droplet Median Volume Diameter (MVD) Effects on Ice Shapes

Jen-Ching Tsao and David N. Anderson
Ohio Aerospace Institute, Brook Park, Ohio

The NASA STI Program Office . . . in Profile

Since its founding, NASA has been dedicated to the advancement of aeronautics and space science. The NASA Scientific and Technical Information (STI) Program Office plays a key part in helping NASA maintain this important role.

The NASA STI Program Office is operated by Langley Research Center, the Lead Center for NASA's scientific and technical information. The NASA STI Program Office provides access to the NASA STI Database, the largest collection of aeronautical and space science STI in the world. The Program Office is also NASA's institutional mechanism for disseminating the results of its research and development activities. These results are published by NASA in the NASA STI Report Series, which includes the following report types:

- TECHNICAL PUBLICATION. Reports of completed research or a major significant phase of research that present the results of NASA programs and include extensive data or theoretical analysis. Includes compilations of significant scientific and technical data and information deemed to be of continuing reference value. NASA's counterpart of peer-reviewed formal professional papers but has less stringent limitations on manuscript length and extent of graphic presentations.

- TECHNICAL MEMORANDUM. Scientific and technical findings that are preliminary or of specialized interest, e.g., quick release reports, working papers, and bibliographies that contain minimal annotation. Does not contain extensive analysis.

- CONTRACTOR REPORT. Scientific and technical findings by NASA-sponsored contractors and grantees.

- CONFERENCE PUBLICATION. Collected papers from scientific and technical conferences, symposia, seminars, or other meetings sponsored or cosponsored by NASA.

- SPECIAL PUBLICATION. Scientific, technical, or historical information from NASA programs, projects, and missions, often concerned with subjects having substantial public interest.

- TECHNICAL TRANSLATION. English-language translations of foreign scientific and technical material pertinent to NASA's mission.

Specialized services that complement the STI Program Office's diverse offerings include creating custom thesauri, building customized databases, organizing and publishing research results . . . even providing videos.

For more information about the NASA STI Program Office, see the following:

- Access the NASA STI Program Home Page at *http://www.sti.nasa.gov*

- E-mail your question via the Internet to help@sti.nasa.gov

- Fax your question to the NASA Access Help Desk at 301–621–0134

- Telephone the NASA Access Help Desk at 301–621–0390

- Write to:
  NASA Access Help Desk
  NASA Center for AeroSpace Information
  7121 Standard Drive
  Hanover, MD 21076

Additional Study of Water Droplet Median Volume Diameter (MVD) Effects on Ice Shapes

Jen-Ching Tsao and David N. Anderson
Ohio Aerospace Institute, Brook Park, Ohio

National Aeronautics and
Space Administration

Glenn Research Center

August 2005

Acknowledgments

This report contains preliminary findings, subject to revision as analysis proceeds.

Available from

Additional Study of Water Droplet Median Volume Diameter (MVD) Effects on Ice Shapes

Jen-Ching Tsao and David N. Anderson
Ohio Aerospace Institute
Brook Park, Ohio 44142

Abstract

This paper reports the result of an experimental study in the NASA Glenn Icing Research Tunnel (IRT) to evaluate how well the *MVD*-independent effect identified previously might apply to SLD conditions in rime icing situations. Models were NACA 0012 wing sections with chords of 53.3 and 91.4 cm. Tests were conducted with a nominal airspeed of 77 m/s (150 kt) and a number of *MVD*'s ranging from 15 to 100 μm with *LWC* of 0.5 to 1 g/m^3. In the present study, ice shapes recorded from past studies and recent results at SLD and Appendix-C conditions are reviewed to show that droplet diameter is not important to rime ice shape for *MVD* of 30 μm or larger, but for less than 30 μm drop sizes a rime ice shape transition from convex to wedge to spearhead type ice shape is observed. Discussion on what may cause such transition is given and some evidence presented in this study suggests that the shape transition could be governed either by the accumulation parameter A_c alone or by β_0 and A_c together.

Nomenclature

A_c	Accumulation parameter, dimensionless
AOA	Angle of attack, °
b	Relative heat factor, dimensionless
c	Airfoil chord, cm
c_p	Specific heat of air, cal/g K
$c_{p,ws}$	Specific heat of water at the surface temperature, cal/g K
d	Cylinder diameter or twice the leading-edge radius of airfoil, cm
h_c	Convective heat-transfer coefficient, cal/s m^2 K
h_G	Gas-phase mass-transfer coefficient, g/s m^2
K	Inertia parameter, dimensionless
K_0	Modified inertia parameter, dimensionless
LWC	Cloud liquid-water content, g/m^3
MVD	Water droplet median volume diameter, μm
n	Freezing fraction, dimensionless
n_0	Stagnation freezing fraction, dimensionless
p	Pressure, Nt/m^2
p_w	Vapor pressure of water in atmosphere, Nt/m^2
p_{ww}	Vapor pressure of water at the icing surface, Nt/m^2
r	Recovery factor, dimensionless
Re	Reynolds number of model, dimensionless
Re_δ	Reynolds number of water drop, dimensionless
SLD	Super-cooled large droplet
s	Distance along airfoil surface measured from stagnation line, cm
t_f	Freezing temperature, °C
t_s	Surface temperature, °C
t	Air temperature, °C
T	Absolute air temperature, K
V	Air velocity, m/s
We	Weber number based on droplet size and water properties, dimensionless
We_c	Weber number based on model size and air properties, dimensionless
We_L	Weber number based on model size and water properties, dimensionless
β_0	Collection efficiency at stagnation line, dimensionless
ϕ	Droplet energy transfer parameter, °C
λ	Droplet range, m
λ_{Stokes}	Droplet range if Stokes Law applies, m
Λ_f	Latent heat of freezing, cal/g
Λ_v	Latent heat of condensation, cal/g
μ	Air viscosity, g/m s
θ	Air energy transfer parameter, °C
ρ	Air density, g/m^3
ρ_i	Ice density, g/m^3
ρ_w	Liquid water density, g/m^3
σ	Surface tension of water over air, dyne/cm
τ	Accretion time, min

Subscripts

|	
st	static
tot	total

<u>Introduction</u>

Recent SLD-to-Appendix C scaling studies in the IRT[1,2] have provided some important information as to how effectively existing scaling methods can be applied to scale SLD drop sizes to Appendix-C conditions. The test results showed that, within the IRT current capability in the SLD regime, good scaling can be achieved by matching scale and reference values of the parameters n_0 and We_L and the product $\beta_0 A_c$, provided model size ratios were limited to 3.4:1 and freezing fractions covered the range from 0.3 to 0.5. Some of the results are reproduced in Figure 1.

It was also found that main ice shapes appear to be independent of *MVD*. Figure 2 shows ice shapes obtained by Chen[3] from a 61-cm-chord GLC 305 airfoil model test in the IRT in 1998 for *MVD* of 55 and 20 μm at freezing fractions of 0.3 and 0.5. At each freezing fraction, the values of A_c, n_0, ϕ, θ and *Re* were maintained constant as drop size decreased. Although β_0 changed from about 92 to 74%, there was no measurable effect of reducing *MVD* on the main ice shape. Similar results were observed later by the authors for NACA 0012 airfoil model tests in the IRT. Figure 3(a) shows ice shapes obtained with 200 and 40 μm drop sizes at 51 m/s for the 53-cm model, and 3(b) compares a *MVD* of

200 μm ice shape with that of 20μm at 77 m/s for the 91-cm model. For each of the comparisons, the main ice shape was little changed by the reduction in *MVD* from SLD conditions to an Appendix-C value. These results suggest that it is possible within the range of test conditions given here to simulate SLD conditions with Appendix-C drop sizes, if the main ice shape is of primary interest.

However, two distinct features of those SLD ice shapes should be noted. First, when drop sizes were larger than 100 μm, the feather structures aft of the main ice shape were significantly larger than those of the Appendix-C shapes. These large feathers were particularly prominent for a *MVD* of 200 μm. Second, the icing limit has changed with *MVD* (i.e. with β_0) because the SLD collection efficiency was so much larger than that for Appendix-C conditions. The SLD ice shapes featured small feathers well aft of the Appendix-C icing limits.

It is not easy to determine the exact conditions for large feather formation and the physics behind them in an icing tunnel environment. But this information is important if one wants to know whether they can be simulated in small-droplet accretions. At rime conditions (i.e. $n_0 = 1$) the ice growth rate is mainly controlled by
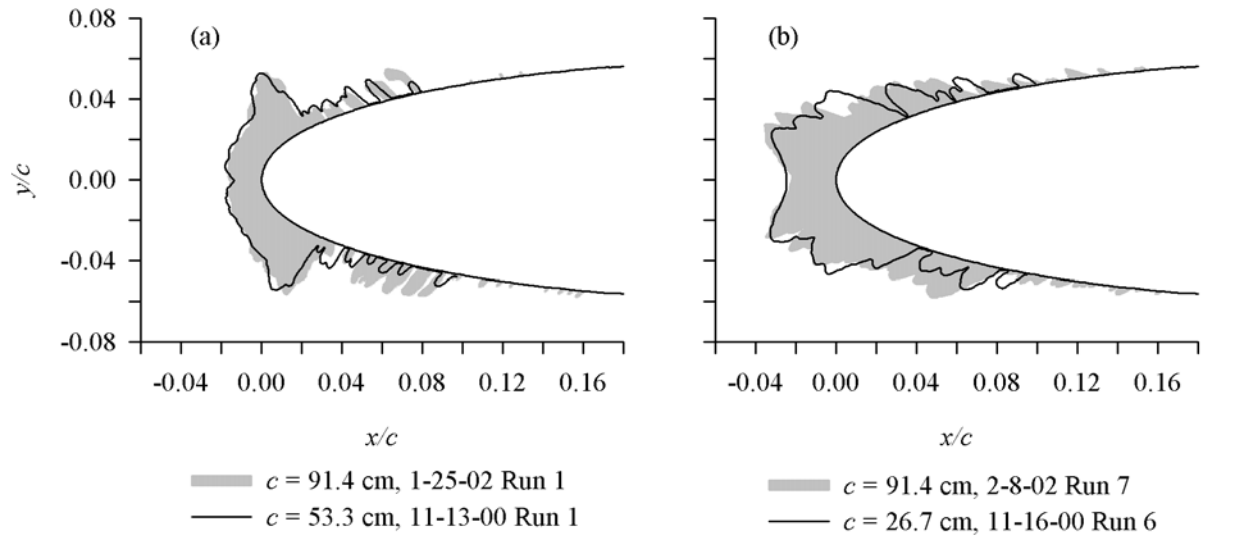

(a) Model Chord Scaled from 91 to 53 cm; n_0, 0.3. (b) Model Chord Scaled from 91 to 27 cm; n_0, 0.5.

Date/Run	c, cm	t_{st}, °C	V, m/s	MVD, μm	LWC, g/m³	τ, min	β_0, %	A_c	n_0	b	ϕ, °C	θ, °C	Re, 10^4	We, 10^3	We_c, 10^3	We_L, 10^6
(a) 1-25-02/1	91.4	-11	51	160	1.50	9.7	95.4	1.70	0.30	1.26	11.1	16.0	11.6	6.50	1.52	1.17
11-13-00/1	53.3	-7	67	38	1.00	7.3	84.9	1.88	0.28	0.58	6.6	9.0	8.6	2.61	1.47	1.15
(b) 2-8-02/7	91.4	-19	52	160	1.50	9.7	95.4	1.70	0.50	1.25	18.9	25.9	12.4	6.54	1.58	1.18
11-16-00/6	26.7	-14	110	21	0.91	2.4	85.8	1.88	0.52	0.49	12.2	14.2	7.0	3.96	1.95	1.57

Figure 1. Examples of Scaling from SLD Conditions to Appendix C. NACA 0012 Airfoils Tested in NASA Glenn Icing Research Tunnel at 0° AOA.[2]
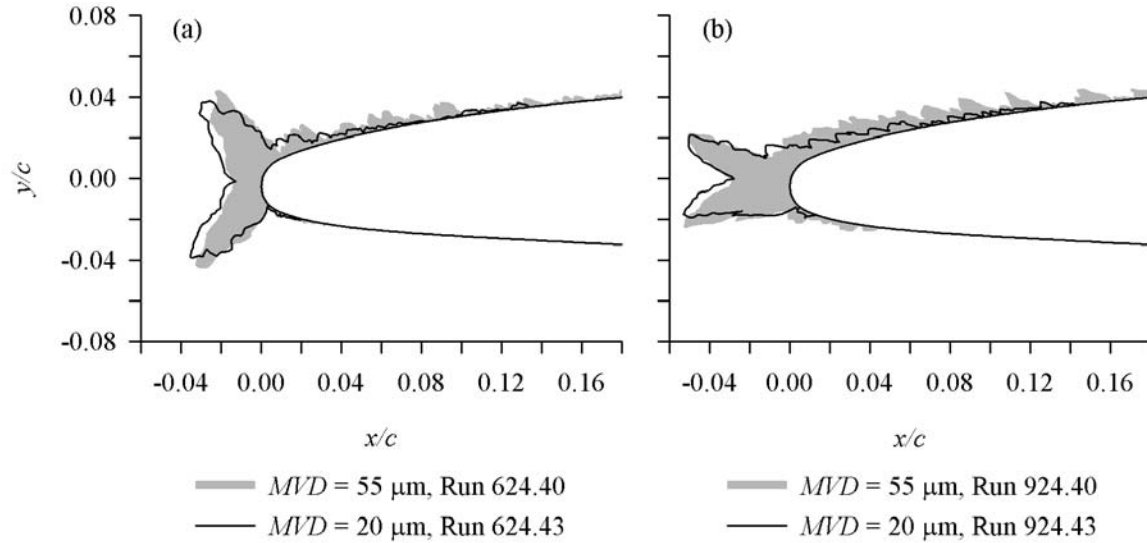
(a) $n_0 = 0.28$ (b) $n_0 = 0.52$

Run	c, cm	t_{st}, °C	V, m/s	MVD, μm	LWC, g/m³	τ, min	β_0, %	A_c	n_0	b	ϕ, °C	θ, °C	Re, 10^4	We, 10^3	We_c, 10^3	We_L, 10^6
(a) 624.40	61.0	-10	90	55	1.16	6.1	91.6	2.53	0.28	0.84	8.9	11.3	10.9	6.76	2.49	2.02
624.43	61.0	-10	89	20	1.31	6.1	73.9	2.83	0.30	0.76	8.8	11.2	10.8	2.44	2.44	1.98
(b) 924.40	61.0	-17	90	55	1.16	6.1	91.7	2.53	0.51	0.84	15.9	20.5	11.4	6.77	2.56	2.02
924.43	61.0	-17	89	20	1.30	6.1	74.0	2.83	0.54	0.76	15.8	20.4	11.4	2.46	2.54	2.00

Figure 2. Ice Shapes for MVD's of 55 and 20 μm. 61-cm-Chord GLC 305 Airfoil Tested in NASA Glenn IRT at 0° AOA.[3]

the droplet impingement rate. This rapid freezing feature at rime probably precludes splashing, and rime tests may therefore give some clues about the cause of the very large glaze SLD feathers. If we find that the large feather formations still form even in rime conditions, we would conclude either that splashing does occur in rime or that some other mechanism produces the large feathers. On the other hand, if the large feathers are not present in rime that would be strong evidence both that splashing is absent from rime and that splashing is probably the cause of the large feather features seen in glaze SLD accretions.

Consequently, a study was commenced to record ice shapes produced at rime conditions with drop MVD's ranging from a low of 15 μm to values well into the SLD regime. In the process of performing these tests, unexpected differences in the main ice shape became evident. In this paper, rime ice shapes obtained only for the MVD range of 15 to 100 μm will be presented to illustrate the differences in main ice shape observed. The results of tests with MVD's greater than 100 μm to explore large SLD feathers is beyond the scope of this paper, and plans are to present that information at another time. For the tests to be reported here, two

NACA 0012 airfoil models with chords of 91.4 and 53.3 cm were used at an airspeed of 77 m/s.

Similarity Parameters

The similarity parameters used in this study followed the Ruff[4] method. To be brief, only the final equations for the similarity parameters will be presented here. Interested readers are referred to a recent comprehensive review on icing scaling methods by Anderson and Tsao[5] for more details.

The modified inertia parameter, K_0, was defined by Langmuir and Blodgett:[6]

$$K_0 = \frac{1}{8} + \frac{\lambda}{\lambda_{Stokes}}\left(K - \frac{1}{8}\right) \qquad (1)$$

In equation (1), K is the inertia parameter,

$$K = \frac{\rho_w\, MVD^2\, V}{18\, d\, \mu} \qquad (2)$$

For cylinders, the cylinder radius should be used in place of d in eq. (2). For airfoils, d is twice the leading-edge radius of curvature. For subsequent equations, d represents either the diameter for cylinders or twice the
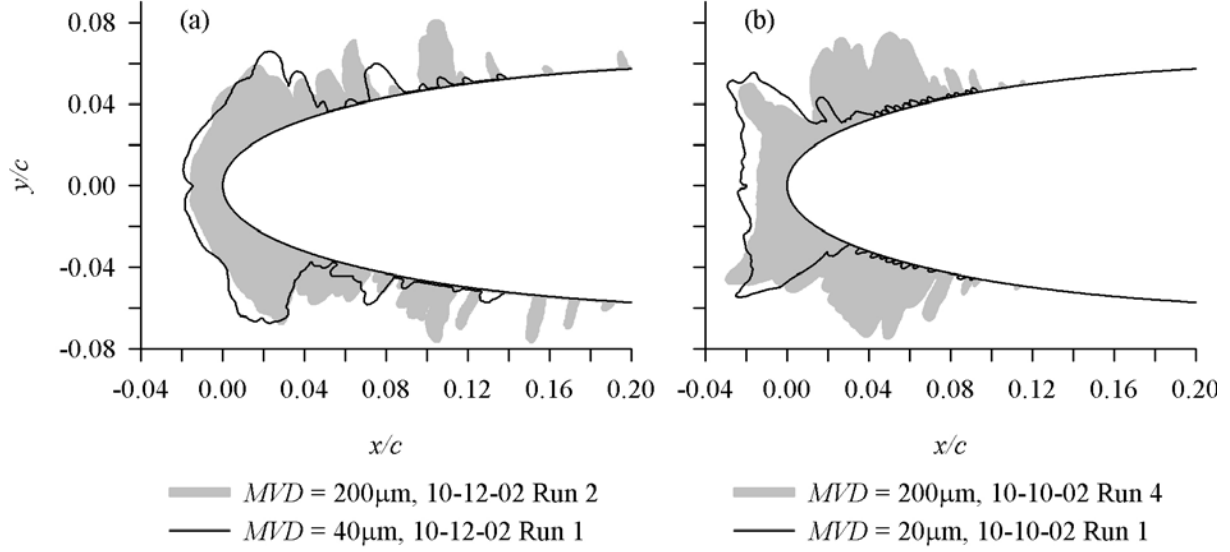
(a) MVD, 200 and 40μm; c, 53.3 cm; V, 51 m/s. (b) MVD, 200 and 20μm; c, 91.4 cm; V, 77 m/s.

Date/Run	c, cm	t_{st}, °C	V, m/s	MVD, μm	LWC, g/m³	τ, min	β_0, %	A_c	n_0	b	ϕ, °C	θ, °C	Re, 10^4	We, 10^3	We_c, 10^3	We_L, 10^6
(a) 10-12-02/2	53.3	-8	51	200	1.20	7.1	97.8	1.71	0.32	0.70	8.1	11.9	6.7	8.13	0.88	0.69
10-12-02/1	53.3	-6	51	40	1.13	10.8	84.0	2.44	0.28	0.57	6.1	9.0	6.6	1.62	0.87	0.68
(b) 10-10-02/4	91.4	-10	77	200	0.86	11.4	97.1	1.71	0.32	0.81	9.5	12.7	17.1	18.38	3.36	2.66
10-10-02/1	91.4	-8	77	20	1.15	17.0	61.1	3.39	0.27	0.68	7.3	9.7	16.8	1.82	3.30	2.63

Figure 3. Comparisons of Ice Shapes from Appendix-C and 200-μm Sprays. NACA 0012 Airfoils Tested in NASA Glenn Icing Research Tunnel at 0° AOA.[2]

leading-edge radius for airfoils. For the NACA 0012 airfoil model, a leading-edge radius of 0.0158c was used (see Abbott and von Doenhoff[7]), where c is the model chord. λ/λ_{Stokes} is the droplet range parameter, defined as the ratio of actual droplet range to that if Stokes drag law for solid-spheres applied. It is a function only of the droplet Reynolds number, Re_δ.

$$Re_\delta = \frac{V\,MVD\,\rho}{\mu} \qquad (3)$$

Langmuir and Blodgett's tabulation of the range parameter was fit to the following expression for this study:

$$\frac{\lambda}{\lambda_{Stokes}} = \left(\begin{array}{c} 0.8388 + 0.001483\,Re_\delta \\ +0.1847\sqrt{Re_\delta} \end{array} \right)^{-1} \qquad (4)$$

Of more practical interest than K_0 is the collection efficiency at the stagnation point, β_0, which was shown by Langmuir and Blodgett to be a function only of K_0,

$$\beta_0 = \frac{1.40\left(K_0 - \frac{1}{8}\right)^{.84}}{1 + 1.40\left(K_0 - \frac{1}{8}\right)^{.84}} \qquad (5)$$

The accumulation parameter is:

$$A_c = \frac{LWC\,V\,\tau}{d\,\rho_i} \qquad (6)$$

If all the water impinging on the leading edge freezes at that location and the leading-edge collection efficiency is 100%, A_c is a measure of the normalized thickness of ice that will accrete.

The freezing fraction is defined as the ratio of the mass of water that freezes at a given location on the surface to the total mass of water that impinges the surface at that location. From Messinger's[8] steady-state surface energy balance formulation, the freezing fraction is

$$n = \frac{c_{p,ws}}{\Lambda_f}\left(\phi + \frac{\theta}{b}\right) \qquad (7)$$

The individual terms in this expression are ϕ, the water energy transfer parameter,

$$\varphi = t_f - t_{st} - \frac{V^2}{2c_{p,ws}} \qquad (8)$$

θ, the air energy transfer parameter,

$$\theta = \left(t_s - t_{st} - r\frac{V^2}{2c_p} \right) + \frac{h_G}{h_c} \left(\frac{\dfrac{p_{ww}}{T_{st}} - \dfrac{p_{tot}}{T_{tot}}\dfrac{p_w}{p_{st}}}{\dfrac{1}{.622}\dfrac{p_{tot}}{T_{tot}} - \dfrac{p_{ww}}{T_{st}}} \right) \Lambda_v \quad (9)$$

and b, the relative heat factor, introduced by Tribus, et. al.[9]

$$b = \frac{LWC\, V\, \beta_0\, c_{p,ws}}{h_c} \quad (10)$$

Equation (9) given by Ruff includes compressibility effects. Simpler forms without compressibility have also been used by Charpin and Fasso[10] and others, but the differences in values are not significant. For the present study the freezing fraction at stagnation, n_0, will be used. At stagnation the recovery factor, r, in equation (9) is unity.

For completeness, the additional similarity parameters used in scaling studies will be given here. They are the Reynolds number for the model, Re, the droplet Weber number, We, the model Weber number using air density, We_c, and the Weber number based on model size and water density, We_L[2]

$$Re = \frac{Vd\rho}{\mu} \quad (11)$$

$$We = \frac{V^2 MVD \rho_w}{\sigma} \quad (12)$$

$$We_c = \frac{V^2 d\rho}{\sigma} \quad (13)$$

$$We_L = \frac{V^2 d\rho_w}{\sigma} \quad (14)$$

Test Description

The icing tests were performed in the NASA Glenn Icing Research Tunnel (IRT). The IRT is a closed-loop, refrigerated, sea-level tunnel with a 1.8 m by 2.7 m rectangular test section. It uses 10 spray bars, a configuration in operation since 1998, to generate a cloud of super-cooled water droplets. The Appendix-C cloud calibration used for these tests was performed in the summer of 2000.[11]

The SLD calibration used in this study was made in the summer of 2002 applying the same methods as the Appendix C. At the time of the tests reported here, only a few specific *MVD-LWC* conditions for speeds of 51, 77 and 103 m/s (i.e. 100, 150 and 200 kt) had been calibrated. Therefore SLD tests were limited to these particular conditions.

The models used were NACA 0012 airfoil sections with chords of 91.4, 53.3 and 26.7 cm. The 91.4-cm-chord airfoil is pictured in figure 4 (a). It was a full-span, fiberglass model. The 53.3-cm-chord model was of 61-cm span and made of aluminum. It was mounted vertically between splitter plates at the center of the IRT test section as shown in figure 4(b). Horizontal lines at the leading edge indicated tunnel center, ±2.5 cm and ±5 cm from the center as visual guides for locating ice tracings. All tests were run at 0° AOA although the mounting system allowed rotation of the model for any given angle of attack setting. Also because of the quick start capability of the current IRT spray system, the models were not shielded during the initiation of the spray.

In preparing for a test, the temperature and airspeed in the test section and the air and water pressures on the spray manifolds were set. When these conditions had stabilized, the spray nozzle valves were opened to initiate the spray. The spray was timed for the required duration, and then turned off. The fan was brought to a full stop and the researchers entered the test section to record the ice shape through hand tracings and photographs. A thin heated stainless plate with a cutout in the shape of the airfoil leading-edge region was inserted into the ice to melt a thin slice down to the model surface. A cardboard template was placed into this gap and an outline of the ice shape traced. Tracings were taken at the vertical center of the tunnel (91 cm from the floor) and at 2.5 cm above the center. The tracings were digitized and the *x-y* coordinates for each ice shape recorded. Subsequently the coordinates were normalized by the model chord for comparison of ice shapes.

Results from test entries in 2002 and 2003 will be presented. Since the shape differences between the two tracing locations were never significant, only centerline shapes will be reported here.

Uncertainty Analysis

Estimates of the uncertainty in the reported average conditions were made by considering inherent errors of instruments, temporal fluctuation and spatial variation of the instrument readings in the test section, and uncertainty in tunnel calibration of *MVD* and *LWC*. Total air temperature was believed to be good to ±0.5°C, and the uncertainty in air velocity was estimated to be ±1m/s. For Appendix-C conditions the net uncertainty in *MVD* was estimated at ±12%. For SLD conditions it may have been as much as ±20%. These uncertainties are not referenced to an absolute value of *MVD*, which is unknown. Repeatability and scatter in the *LWC* calibration data suggests the uncertainty is about ±12% for both Appendix-C and SLD conditions.

(a) 91.4-cm-Chord NACA 0012 Model Installed in IRT Test Section.

(b) 53.3-cm-Chord NACA 0012 Model Installed in IRT Test Section.

Figure 4. Model Description.

These uncertainties in the test parameters were used to estimate the following uncertainties in the similarity parameters for the Appendix-C tests: 9% in β_0, 12% in A_c, 13% in n_0, 3% in Re, 13% in We and 5% in We_L. For the SLD tests the uncertainties were: 3% in β_0, 12% in A_c, 11% in n_0, 3% in Re, 21% in We and 5% in We_L.
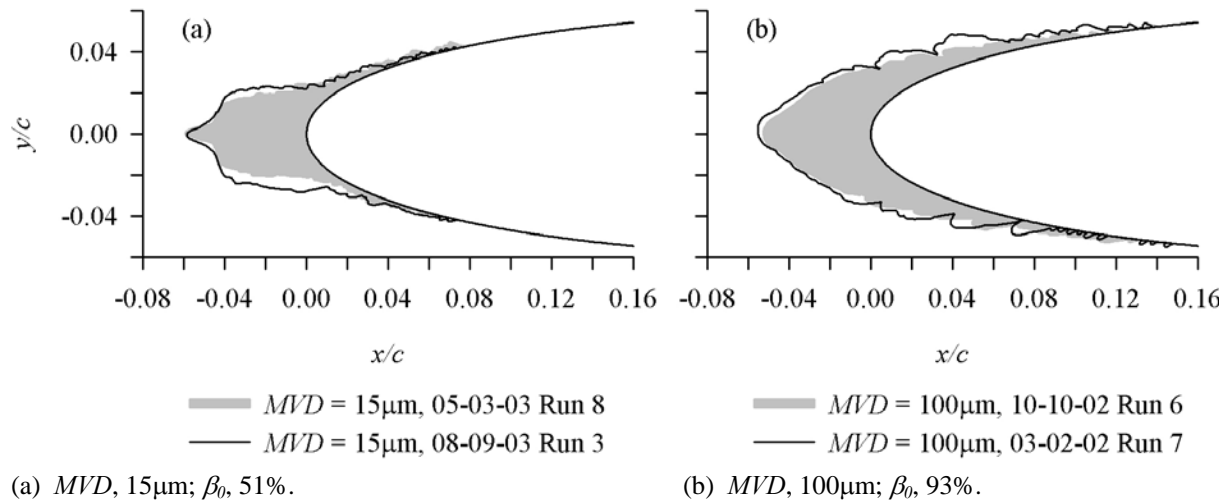
<u>Results</u>

<u>IRT Repeatability</u>

Rime icing tests were made over a number of MVD's, chord sizes and airspeeds while maintaining constant $\beta_0 A_c$. They provide a good check on tunnel LWC calibrations. Figure 5 compares ice shapes obtained at different entry dates for MVD's of 15 μm (5(a)) and 100 μm (5(b)). Average recorded test conditions and corresponding similarity parameters for each of the tests are given in a table accompanying the figure. Temperatures were calculated to provide just rime icing conditions (i.e. the warmest temperature permitted for rime). Because the recorded conditions may be slightly different from the planned values for each test, the similarity parameters intended to be maintained may not always have matched exactly. The differences observed in the ice shapes were well within the uncertainty in LWC; therefore, these results provide confidence that the IRT test conditions are repeatable for both SLD and Appendix-C conditions.

<u>The Change of Rime Ice Shape</u>

Rime ice shapes do not all have the same profile. The shapes shown in figure 5(a) for 15 μm sprays are noticeably different from those shown in figure 5(b) for 100 μm. Both were obtained with the 91-cm-chord NACA 0012 model at a velocity of 77 m/s. Spray conditions for all the test results shown produce rime ice ($n_0 = 1$) with the same leading-edge ice thickness (i.e., $\beta_0 A_c$ the same). Because of the different drop sizes, the values of β_0 for the two sets of test are significantly different: about 51% for the 15-μm case and 93% for 100 μm. For a constant $\beta_0 A_c$, this change in β_0 requires that the 15-μm tests be run at an A_c nearly double that for the 100-μm.

The 15-μm MVD cloud produces a spearhead-like rime ice shape shown in Figure 5(a). It features a small ice ridge of relatively compact ice at the center with adjacent regions of long rime feathers growing into the flow direction to form relatively flat shoulders. Near the aft extent of those long feathers, a sudden transition to a region with much smaller and sparsely distributed feathers is observed extending back toward the icing limit. The shape and features were found to be repeatable for different values of LWC, as shown in figure 5(a). For the conditions of run 8 on 5-3-03, a temperature of –23°C would have been cold enough to produce

	(a) MVD = 15μm, 05-03-03 Run 8	(b) MVD = 100μm, 10-10-02 Run 6
	MVD = 15μm, 08-09-03 Run 3	MVD = 100μm, 03-02-02 Run 7

(a) *MVD*, 15μm; β_0, 51%. (b) *MVD*, 100μm; β_0, 93%.

Date/Run	c, cm	t_{st}, °C	V, m/s	MVD, μm	LWC, g/m³	τ, min	β_0, %	$\beta_0 A_c$	n_0	b	ϕ, °C	θ, °C	Re, 10^4	We, 10^3	We_c, 10^3	We_L, 10^6
(a) 5-3-03/8	91.4	-26	77	15	1.00	20.3	51.1	1.82	1.0	0.50	25.5	32.4	18.9	1.37	3.55	2.65
8-9-03/3	91.4	-21	77	15	0.50	40.8	51.0	1.82	1.0	0.25	20.6	26.9	18.1	1.36	3.42	2.61
(b)10-10-02/6	91.4	-26	77	100	0.68	16.4	93.2	1.82	1.0	0.61	25.6	32.5	19.1	9.16	3.59	2.63
3-2-02/7	91.4	-26	77	100	0.68	16.4	93.2	1.81	1.0	0.61	25.7	32.6	19.1	9.16	3.59	2.63

Figure 5. Repeated Rime Ice Shapes for *MVD*'s of 15 and 100 μm. 91-cm-Chord NACA 0012 Airfoil at 0° AOA.

rime, and other tests performed at this temperature gave results consistent with those of figure 5(a). The fact that the decrease in temperature to –26°C made no change in the appearance of the ice assures us that the shapes of figure 5(a) represent fully rime ice. Similar spearhead ice shapes have been observed and reported by Brunet and Guffond[12] on cylinders.

In contrast, figure 5(b) shows a convex type rime ice shape for the 100-μm droplet *MVD*. The ice shape conforms roughly to the leading-edge contour of the model with some small rime feathers (pointing into the flow direction) on the ice surface near the icing limits.

Understanding the physics behind the different shapes produced for rime conditions is a necessary step toward insuring that scaling methods include the most significant factors affecting ice shape. Scaling methods developed without a complete understanding may work well for tested conditions but be deficient for other situations not evaluated during method development. One step to understanding is to identify ranges of conditions for which different shapes occur. Additional rime ice shapes obtained from the same model and velocity as for figure 5 with intermediate *MVD* of 20, 30 and 70 μm were examined and shown in figure 6. Two observations are noted. First, the convex type rime ice shape is maintained for *MVD* of 30 μm or larger. Second, there is a shape transition for *MVD* less than 30 μm from **(1)** a convex type rime ice shape to **(2)** a wedge-like rime ice shape for a 20-μm *MVD* cloud,

then to **(3)** a spearhead-like rime ice shape for a smaller *MVD* of 15 μm. In the transition, the large feather structures seem to become more important and relevant in developing the final ice shape. Close-up pictures of a 15-μm (spearhead type) and a 30-μm (convex type) rime ice shapes are provided in figures 7 and 8 for visualization purpose, and they show some span-wise variations in features, possibly due to cloud non-uniformity effects that can not be fully captured by the 2D tracing.

Finally, another series of rime ice shapes were examined. These were obtained at the same velocity as for figures 5 – 8, but with a smaller model (53.3-cm chord). The results are given in figure 9. Due to the smaller model size used, the β_0 values for each drop size are higher than the corresponding values for figure 6. Now the 15-μm *MVD* (figure 9 (a)) no longer shows a spearhead shape, but rather a wedge shape very much like the 20-μm test of figures 6 (a) and 9 (a). Drop sizes of 30 and 70 μm (figure 9 (b)), produced the same convex shapes observed for the larger model in figures 5 (b) and 6 (b).

It is reasonable at first to speculate that the rime ice shape transition from the convex shapes of figures 5 (b), 6 (b) and 9 (b) to the wedge (figure 9 (a) and the 20-μm shape of 6 (a)), then to the spearheads (figure 5 (a) and the 15-μm shape of 6 (a)) is a function of the stagnation collection efficiency β_0 and the corresponding β distribution on the model surface. If the change
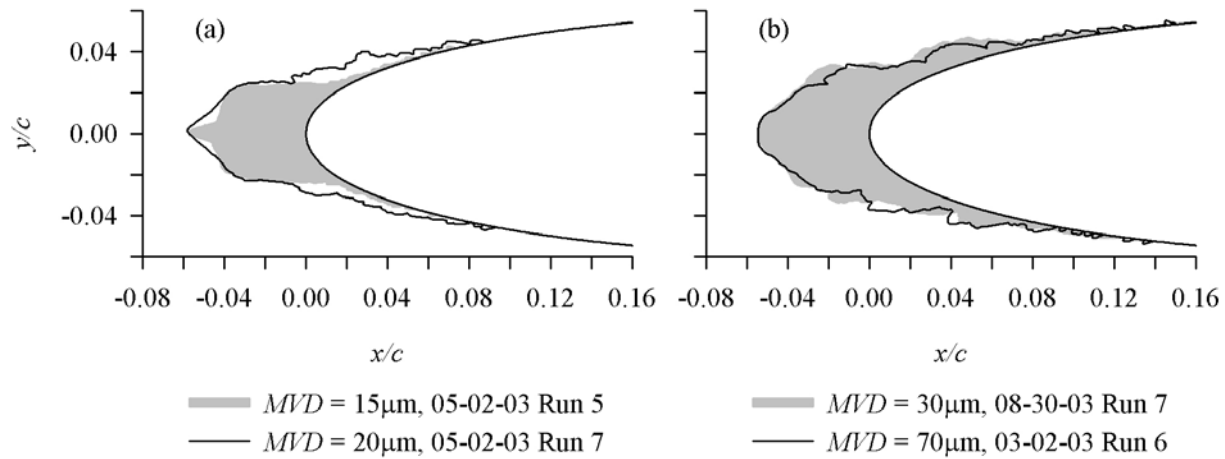
(a) Shapes for 15- and 20-µm *MVD* Spray.   (b) Shapes for 30- and 70-µm *MVD* Spray.

Date/Run	c, cm	t_{st}, °C	V, m/s	MVD, µm	LWC, g/m³	τ, min	β_0, %	$\beta_0 A_c$	n_0	b	ϕ, °C	θ, °C	Re, 10^4	We, 10^3	We_c, 10^3	We_L, 10^6
(a) 5-2-03/5	91.4	-22	77	15	1.00	20.3	51.0	1.81	1.0	0.50	21.8	28.2	18.3	1.36	3.44	2.62
5-2-03/7	91.4	-26	77	20	1.00	16.9	61.3	1.81	1.0	0.60	25.1	31.9	18.7	1.83	3.51	2.63
(b) 8-30-03/7	91.4	-21	77	30	0.65	21.7	73.2	1.80	1.0	0.46	20.6	26.8	18.3	2.72	3.48	2.63
3-2-02/6	91.4	-23	77	70	0.60	19.3	89.6	1.81	1.0	0.52	22.7	29.2	18.8	6.41	3.55	2.63

**Figure 6.** Rime Ice Shapes for *MVD*'s of 15 to 70 µm. 91.4-cm NACA 0012 Airfoil at 0° AOA.

of rime ice shapes is correlated with the initial stagnation collection efficiency, β_0, the present results would suggest that the rime ice shape is of convex type when $\beta_0 > 0.8$, wedge type when $0.6 < \beta_0 < 0.8$, and spearhead type when $\beta_0 < 0.6$.

To see how the β profile might differ for the 15- and 100-µm shapes of figure 5, some calculations were made using LEWICE 2.2[13] for a clean 91.4-cm NACA 0012 airfoil model. A simple monodisperse cloud was utilized. The numerical results, see figure 10, show that as the *MVD* decreases from 100 µm to 15 µm, the β curve is reduced in both magnitude and extent (impingement limits) on the model surface. The β_0 value has dropped almost by half (from 0.93 to 0.51) and the impingement limits have been reduced by a factor of four.

The most striking difference in the two collection efficiency curves is the narrowness of the 15-µm plot compared with that for 100 µm. This characteristic suggests that, in the absence of feathers and assuming the shape of the β curve does not change as ice accretes, ice would tend to form in only a very narrow region on the leading edge of the model, thus producing a spearhead. However, as ice accretes on the model, the resulting ice-shape change will influence both the shape of the β profile and the value of β_0. Brunet and Guffond presented photographs to illustrate how the shape of ice formations on cylinders changes with time as ice continues to accrete. Brunet and Guffond's ice shapes evolved from a convex shape similar to those of figures 5 (b), 6 (b) and 9 (b), to a wedge-like shape like those in 9 (a) and the 20-µm shape in 6 (a), then to a spearhead ice shape closely resembling those of the 15-µm tests in figures 5 (a) and 6 (a). Although Brunet and Guffond did not provide conditions for these tests, the ice they show has the appearance of rime.

The Brunet and Guffond results demonstrate the importance of accretion time (or effectively the accumulation parameter A_c) on ice-shape characteristics. There is, of course, an interaction between the rime ice shape at any time and the collection efficiency. The changing nature of the ice shape creates a time-dependence in the collection efficiency, which in turn influences the evolving rime shape. As noted previously, the present tests were made with a constant value of the product $\beta_0 A_c$, to insure that the leading-edge accretions would be the same size. Thus, as β_0 decreased, A_c had to be increased to compensate. Consequently, it is difficult to separate the effects of collection efficiency and accumulation parameter on the developing ice shape. Additional testing is needed to record accretions with small droplets over a range of values of A_c and also to look at larger droplets with greater values of A_c than tested in this investigation. Such a study would help to determine how the shape transition process (i.e. convex-wedge-spearhead) correlates with A_c and β_0.
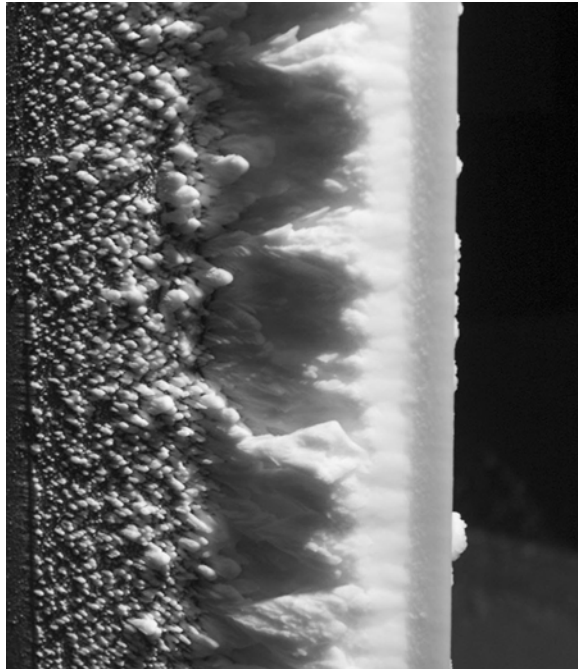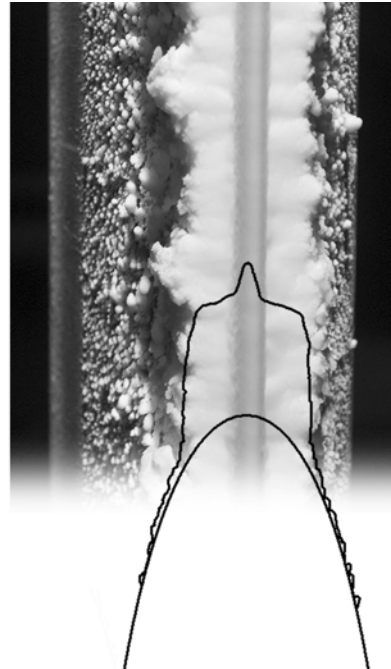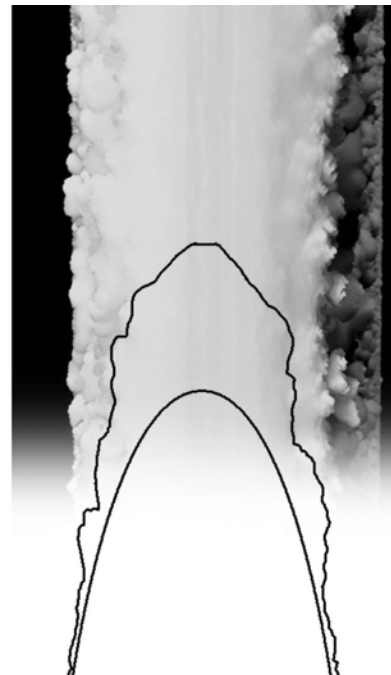
(a) Side View.   (b) Front View with Profile Tracing.

Figure 7. Rime Ice on 91-cm-Chord NACA 0012 for *MVD* = 15 μm. Test of 5-2-03 Run 5. See Figure 6 (a) for Conditions.

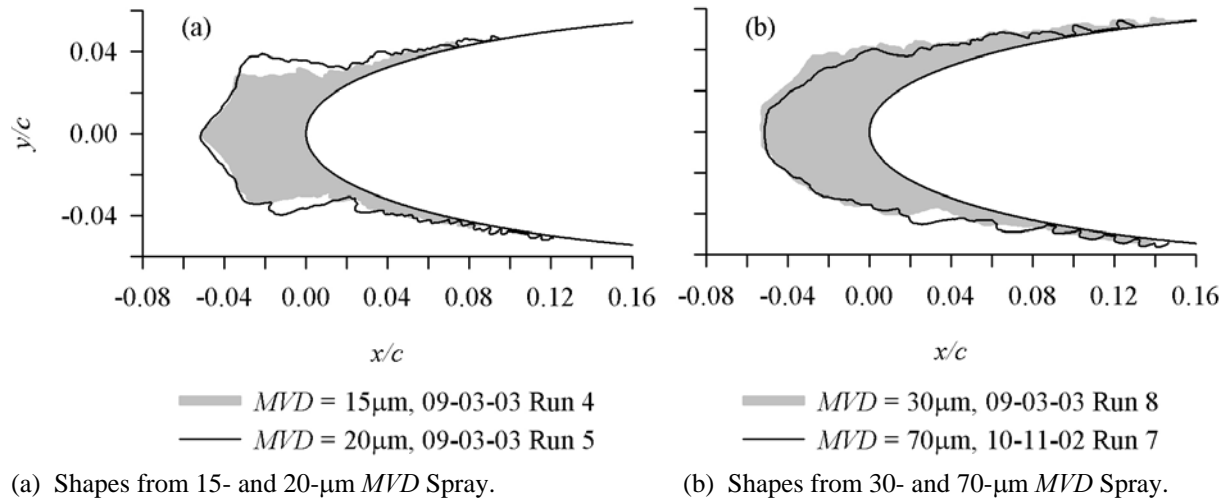

(a) Side View.   (b) Front View with Profile Tracing.

Figure 8. Rime Ice on 91-cm-Chord NACA 0012 for *MVD* = 30 μm. Test of 8-30-03 Run 7. See Figure 6 (b) for Conditions.

the *MVD* by itself can not completely represent the cloud dynamics and its influence on accretions, the actual drop size distribution for different cloud *MVD*'s should be examined. It was shown, for example in the IRT, that the 95% cumulative *LWC* droplet diameter (which is a good estimate of the maximum droplet diameter in the cloud) is about 23 μm for a *MVD* of 15 μm, but is 90 μm for a *MVD* of 20 μm and 260 μm for a *MVD* of 100 μm. Thus, as *MVD* increases the droplet size distribution becomes broader. It is possible that these distribution differences for various cloud *MVD*'s have an effect on the rime ice shapes. If so, the effect on shape can be expected to apply to glaze conditions, as well as to rime.

For glaze icing in SLD conditions, splashing may also have an important effect on ice shape. For conditions for which splashing is important, a new way of representing the cloud to better characterize the effects of the varying momenta of different drop sizes may be needed.

Finally, there is another factor to be considered for the rime ice shape transition. That is the drop size distribution for different cloud *MVD*'s. Since it is known that

(a) Shapes from 15- and 20-μm *MVD* Spray.

(b) Shapes from 30- and 70-μm *MVD* Spray.

Date/Run	c, cm	t_{st}, °C	V, m/s	MVD, μm	LWC, g/m³	τ, min	β_0, %	$\beta_0 A_c$	n_0	b	ϕ, °C	θ, °C	Re, 10^4	We, 10^3	We_c, 10^3	We_L, 10^6
(a) 9-3-03/4	53.3	-12	77	15	0.50	19.4	62.7	1.82	1.0	0.23	11.6	15.7	10.0	1.38	1.96	1.55
9-3-03/5	53.3	-14	77	20	0.50	16.9	71.6	1.82	1.0	0.27	13.0	17.6	10.1	1.84	1.96	1.54
(b) 9-3-03/8	53.3	-19	77	30	0.65	11.4	81.4	1.82	1.0	0.39	18.1	23.9	10.4	2.76	2.01	1.55
10-11-02/7	53.3	-20	77	70	0.60	10.8	93.1	1.82	1.0	0.41	18.9	24.8	10.7	6.41	2.04	1.54

Figure 9. Rime Ice Shapes for *MVD*'s of 15 to 70 μm. 53.3-cm NACA 0012 Airfoil at 0° AOA.

Concluding Remarks

Ice shape comparisons were made for NACA 0012 airfoil models with chords of 53.3 and 91.4 cm. Test conditions were set so that rime ice would be obtained
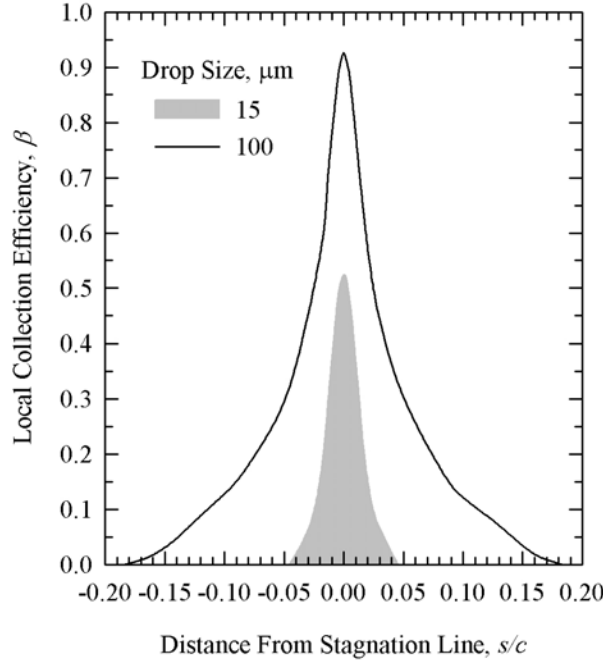
Figure 10. Effect of *MVD* on Collection Efficiency. β from LEWICE[13] for Clean 91-cm-Chord NACA 0012 Airfoil at 0° AOA. t_{st}, -33°C; V, 77 m/s.

ditions were set so that rime ice would be obtained for a nominal airspeed of 77 m/s, *MVD*'s ranging from 15 to 100 μm and *LWC*'s of 0.5 to 1 g/m³. The product $\beta_0 A_c$ was maintained the same for all tests (thus, the leading-edge ice thickness was the same) to permit direct comparison of ice shapes obtained at different conditions. Important findings and suggestions are summarized as follows.

- For the conditions of this study, a rime ice shape transition from convex to wedge to spearhead type was observed as the *MVD* decreased from 30 to 20 to 15 μm.

- For the conditions of this study, the convex type rime ice shape was maintained for *MVD* of 30 μm or larger. This suggests that it is possible in various rime icing conditions tested here to simulate SLD conditions with Appendix-C drop sizes no less than 30 μm.

- For the conditions of this study, the rime ice shape was of convex type when $\beta_0 > 0.8$, wedge type when $0.6 < \beta_0 < 0.8$, and spearhead type when $\beta_0 < 0.6$.

- Evidence from reference 12 suggests that accretion time (or effectively the A_c) is important in determining the ice shape. Further study of the effect of A_c on the ice shape transition is needed.

- The actual drop size distribution for different cloud *MVD*'s may need to be considered to help explain the shape transition.

References

[1] Anderson, David N., "A Preliminary Study of Ice-Accretion Scaling for SLD Conditions," AIAA-2002-0521, January 2002.

[2] Anderson, David N. and Tsao, J.C., "Additional Results of Ice-Accretion Scaling at SLD Conditions," AIAA-2003-0390, January 2003.

[3] Chen, Shu-Cheng, unpublished GLC 305 icing studies in NASA Glenn IRT, March, April, September and October 1998.

[4] Ruff, G.A., "Analysis and Verification of the Icing Scaling Equations," AEDC-TR-85-30, vol 1 (rev), March 1986.

[5] Anderson, David N. and Tsao, J.C., "Overview of Icing Physics Relevant to Scaling," FAA In-Flight Icing / Ground De-icing International Conference & Exhibition, SAE-2003-01-2130, June 16-20, 2003.

[6] Langmuir, Irving and Blodgett, Katharine B. "A Mathematical Investigation of Water Droplet Trajectories," Army Air Forces Technical Report No. 5418, February 1946.

[7] Abbott, Ira H. and von Doenhoff, Albert E., *Theory of Wing Sections*, Dover, New York, 1959, pp114 and 321.

[8] Messinger, B.L., "Equilibrium Temperature of an Unheated Icing Surface as a Function of Airspeed," *J. Aeron. Sci.*, vol. 20 no. 1, January 1953, pp 29 – 42.

[9] Tribus, Myron, Young, G.B.W. and Boelter, L.M.K., "Analysis of Heat Transfer Over a Small Cylinder in Icing Conditions on Mount Washington," *Trans. ASME*, vol. 70, November 1948, pp 971 – 976.

[10] Charpin, Francois and Fasso, Guy, "Essais de givrage dans la grande soufflerie de Modane sur maquettes a echelle grandeur et echelle reduite," *L'Aeronautique et l'Astronautique*, no. 38, 1972, pp 23 – 31. English translation published as "Icing Testing in the Large Modane Wind-Tunnel on Full-Scale and Reduced Scale Models," NASA TM-75373, March 1979.

[11] Ide, Robert F. and Oldenburg, John R., "Icing Cloud Calibration of the NASA Glenn Icing Research Tunnel," AIAA-2001-0234, January 2001.

[12] Brunet, Luc and Guffond, Didier, "Interpretation of An Experimental Spearhead Shape Ice Formation by Using A Numerical Model," the 4th International Workshop on Atmospheric Icing of Structures at Paris, France, 1988.

[13] Wright, W.B., "LEWICE 2.2 Capabilities and Thermal Validation," AIAA-2002-0383, January 2002.

REPORT DOCUMENTATION PAGE

Form Approved
OMB No. 0704-0188

Public reporting burden for this collection of information is estimated to average 1 hour per response, including the time for reviewing instructions, searching existing data sources, gathering and maintaining the data needed, and completing and reviewing the collection of information. Send comments regarding this burden estimate or any other aspect of this collection of information, including suggestions for reducing this burden, to Washington Headquarters Services, Directorate for Information Operations and Reports, 1215 Jefferson Davis Highway, Suite 1204, Arlington, VA 22202-4302, and to the Office of Management and Budget, Paperwork Reduction Project (0704-0188), Washington, DC 20503.

1. AGENCY USE ONLY *(Leave blank)*	2. REPORT DATE August 2005	3. REPORT TYPE AND DATES COVERED Final Contractor Report

4. TITLE AND SUBTITLE

Additional Study of Water Droplet Median Volume Diameter (MVD) Effects on Ice Shapes

5. FUNDING NUMBERS

WBS–22–728–41–17
NCC3–938

6. AUTHOR(S)

Jen-Ching Tsao and David N. Anderson

7. PERFORMING ORGANIZATION NAME(S) AND ADDRESS(ES)

Ohio Aerospace Institute
22800 Cedar Point Road
Brook Park, Ohio 44142

8. PERFORMING ORGANIZATION REPORT NUMBER

E–15223

9. SPONSORING/MONITORING AGENCY NAME(S) AND ADDRESS(ES)

National Aeronautics and Space Administration
Washington, DC 20546–0001

10. SPONSORING/MONITORING AGENCY REPORT NUMBER

NASA CR—2005–213853
AIAA–2004–0413

12a. DISTRIBUTION/AVAILABILITY STATEMENT

Unclassified - Unlimited
Subject Category: 03

Available electronically at http://gltrs.grc.nasa.gov

This publication is available from the NASA Center for AeroSpace Information, 301–621–0390.

12b. DISTRIBUTION CODE

13. ABSTRACT *(Maximum 200 words)*

This paper reports the result of an experimental study in the NASA Glenn Icing Research Tunnel (IRT) to evaluate how well the MVD-independent effect identified previously might apply to SLD conditions in rime icing situations. Models were NACA 0012 wing sections with chords of 53.3 and 91.4 cm. Tests were conducted with a nominal airspeed of 77 m/s (150 kt) and a number of MVD's ranging from 15 to 100 μm with LWC of 0.5 to 1 g/m^3. In the present study, ice shapes recorded from past studies and recent results at SLD and Appendix-C conditions are reviewed to show that droplet diameter is not important to rime ice shape for MVD of 30 μm or larger, but for less than 30 μm drop sizes a rime ice shape transition from convex to wedge to spearhead type ice shape is observed. Discussion on what may cause such transition is given and some evidence presented in this study suggests that the shape transition could be governed either by the accumulation parameter A_c alone or by β_o and A_c together.

14. SUBJECT TERMS

Icing physics; Scaling; SLD; LWC

15. NUMBER OF PAGES
17

16. PRICE CODE

17. SECURITY CLASSIFICATION OF REPORT Unclassified	18. SECURITY CLASSIFICATION OF THIS PAGE Unclassified	19. SECURITY CLASSIFICATION OF ABSTRACT Unclassified	20. LIMITATION OF ABSTRACT

NSN 7540-01-280-5500

Standard Form 298 (Rev. 2-89)
Prescribed by ANSI Std. Z39-18
298-102